HHS Public Access

Author manuscript

Neuroscience. Author manuscript; available in PMC 2018 March 21.

Published in final edited form as:

Neuroscience. 2014 September 26; 277: 250–266. doi:10.1016/j.neuroscience.2014.07.006.

Bidirectional Modulation of Deep Cerebellar Nuclear Cells Revealed by Optogenetic Manipulation of Inhibitory Inputs from Purkinje Cells

V. Z. Han[1,*], **G. Magnus**[1], **Y. Zhang**[1,2], **A.D. Wei**[1,5], and **E. Turner**[1,3,4]

[1]Center for Integrative Brain Research, Seattle Children's Research Institute Seattle, WA 98101

[2]Department of Pediatrics and Neuroscience, Xijing Hospital, Xi'an 710032, China

[3]Department of Psychiatry and Behavioral Sciences, University of Washington Seattle WA, 98101

[4]Center on Human Development and Disability, University of Washington Seattle WA, 98195

[5]Department of Neurological Surgery, University of Washington, Seattle, WA 98101

Abstract

In the mammalian cerebellum, deep cerebellar nuclear (DCN) cells convey all information from cortical Purkinje cells (PCs) to premotor nuclei and other brain regions. However, how DCN cells integrate inhibitory input from PCs with excitatory inputs from other sources has been difficult to assess, in part due to the large spatial separation between cortical PCs and their target cells in the nuclei. To circumvent this problem we have used a Cre-mediated genetic approach to generate mice in which channelrhodopsin-2 (ChR2), fused with a fluorescent reporter, is selectively expressed by GABAergic neurons, including PCs. In recordings from brain slice preparations from this model, mammalian PCs can be robustly depolarized and discharged by brief photo stimulation. In recordings of postsynaptic DCN cells, photo stimulation of PC axons induces a strong inhibition that resembles these cells' responses to focal electrical stimulation, but without a requirement for the glutamate receptor blockers typically applied in such experiments. In this optogenetic model, laser pulses as brief as 1 ms can reliably induce an inhibition that shuts down the spontaneous spiking of a DCN cell for ~50 ms. If bursts of such brief light pulses are delivered, a fixed pattern of bistable bursting emerges. If these pulses are delivered continuously to a spontaneously bistable cell, the immediate response to such photostimulation is inhibitory in the cell's depolarized state and excitatory when the membrane has repolarized; a less regular burst pattern then persists after stimulation has been terminated. These results indicate that the spiking activity of DCN cells can be bidirectionally modulated by the optically activated synaptic inhibition of cortical PCs.

Correspondence: Victor Z Han, Center for Integrative Brain Research, Seattle Children's Research Institute, 1900 Ninth Avenue, Mail stop: C9S-10, Seattle, WA 98101, Tel: (206) 884-1176, Fax: (206) 884 1210, victor.han@seattlechildrens.org.

Keywords

Purkinje cell; deep nuclear cell; synaptic inhibition; photostimulation; optogenetic model

Introduction

The mammalian cerebellum plays important roles in motor control and motor learning, and is also involved in such non-motor functions as arousal, emotion, and cognition (Ito, 2001; Leiner et al, 1993; Raymond et al, 1996; Stoodley et al, 2012). How such functions are accomplished, either directly by the cerebellum or through its interactions with other brain structures, is not well understood. The fact that its circuitry is remarkably uniform an d well-defined in all its subregions and across many species has suggested that the cerebellum performs a single characteristic computation (Ito, 1984; Voogd and Glickstein, 1998; Apps and Garwicz, 2005). Despite great variation in its inputs, one constant is that the sole output projection of the cerebellar cortex is from the inhibitory Purkinje cells (PCs) to neurons of the deep cerebellar nuclei (DCN) and the vestibular nuclei (VN), where this inhibition is integrated with excitation transmitted by collaterals of mossy and climbing fibers. As DCN cells convey the final cerebellar output signals, how they process synaptic inhibition from PCs is a key factor in determining the result of the cerebellar computation that is sent to premotor and non-motor nuclei in the brainstem and thalamus (Bell et al, 2008; Eccles et al, 1967; Sugihara, 2011; Teune et al, 2000; Welsh et al, 1995).

Despite decades of effort, exactly how PC-DCN neuron interactions occur is far from clear. An outstanding question is how individual DCN cells integrate inhibitory inputs from PCs and excitatory inputs from the brainstem to generate their functional output signals. Such characterization has proved difficult to obtain because PCs and DCN neurons are too far apart in the mammalian cerebellum to allow monosynaptically-connected pairs of neurons to be recorded simultaneously (McDevitt et al, 1987). As an approximation, studies using dynamic clamp to model PC-triggered conductances in DCN neurons have indicated an important role for PC firing synchrony in determining both the responsiveness of DCN cells to input from excitatory terminals and the timing of these cells' post-inhibitory spiking (Jaeger, 2011; Person and Raman, 2012). That the modulation of PC ensemble activity is likely to play a major role in DCN neuronal computation is reinforced by quantitative anatomy, which has demonstrated that each DCN neuron receives synaptic inputs from ~860 PCs (Palkovitz et al, 1977), although there is more recent evidence that this convergence ratio may be more than an order of magnitude less (Person and Raman, 2012). Such real-time synaptic integration within the DCN is believed to be essential to movement coordination. Although an earlier model holds that the activity-dependent modification of synaptic strength, including long-term potentiation (LTP) and depression (LTD), in cortical PCs underlies associative eyeblink conditioning and vestibuloocular reflex (VOR) adaptation (Gao et al, 2012; Hansel et al, 2001; Ito, 2001; Jorntell and Hansel, 2006; Pugh and Raman, 2006), real-time interactions between cortical PCs and DCN cells during movement are also believed to be critically important for motor control and motor learning, as indicated by experimental studies and computational modeling (Mauk and Donegan, 1997; Ohyama et al, 2006; Shutoh et al, 2006).

To further explore and characterize the critical inhibitory synapse between cortical PCs and DCN cells, we have created a mouse model, in which the conditional expression of channelrhodopsin 2 (ChR2), fused with a fluorescent reporter protein, is induced by a $Gad2^{Cre}$ transgene, such that GABAergic neurons, including PCs, can be depolarized by blue light (Madisen et al, 2012; Nagel et al, 2002; Taniguchi et al, 2011; Tye and Deisseroth, 2012). Using cerebellar slices from this model, we have found that brief photo stimulation can robustly depolarize PCs and induce a strong inhibition in DCN cells that is very similar to the IPSPs induced by conventional focal electrical stimulation under pharmacological isolation (Aizenman et al, 1998). We have further shown that the spontaneous firing activity of at least some DCN cells can be effectively modulated by the optical activation of PC axons through the voltage-dependent inhibition, shunting or excitation of the postsynaptic membrane current.

Experimental Procedures

Generation of optogenetic mice for studies of GABAergic PCs

Two parental mouse strains allowing Cre-induced conditional expression of ChR2 from the mouse *Gt(ROSA)26Sor* locus were employed: Ai27, which expresses a ChR2(H134R)-tdTomato fusion protein, and Ai32, which expresses a ChR2(H134R)-EYFP fusion protein (Madisen et al, 2012). These were obtained from Dr. H. Zeng at the Allen Institute for Brain Science. The Cre-driver line $Gad2^{tm2(cre)Zjh/J}$ ($Gad2^{Cre}$) was obtained from Jackson Labs (Taniguchi et al, 2011). The Cre-driver and optogenetic effector transgenic lines were maintained separately on a C57BL/6 genetic background, and were interbred to generate $Gad2^{Cre}$/Ai27 and $Gad2^{Cre}$/Ai32 double-heterozygotes for the experiments described below. It has been well documented that ChR2 is a light-gated nonspecific cation channel expressed in the plasma membranes of target neurons and that it opens on a millisecond timescale upon exposure to blue laser light, leading to the influx of Na^+, K^+, Ca^{2+} and H^+ (Nagel et al, 2002; Madisen et al, 2012). These basic channel properties are also present in the target cells in our model (see below).

Slice preparation

Mice of either sex between P14 and P30 were deeply anesthetized with isoflurane and decapitated. The brain was quickly removed and left in ice-cold oxygenated saline for ~1 min to harden the tissue. After trimming, the cerebellum (with the brainstem attached) was glued to a cutting stage with the back support of an agar block. The cutting tray was filled with oxygenated cold saline (bubbled with 95% O_2 and 5% CO_2) that included (in mM): sucrose 252, KCl 2, $MgCl_2$ 2, $CaCl_2$ 2.6, NaH_2PO_4 1.2, $NaHCO_3$ 26, and glucose 20, with the pH adjusted to 7.4 ± 0.5 and the osmolarity to 315 ± 5 mOsm. After cutting, typically at 200 μm in either the parasagittal or transverse plane, slices were immediately returned to the same solution and maintained in a warm bath (28 ± 0.5° C) for recovery. After 30-60 min, they were transferred into normal oxygenated ACSF with the same contents as before except for the replacement of sucrose by 126 mM NaCl. Slices were kept at room temperature until recording.

Whole-cell patch recording

Individual slices were placed in a submerged recording chamber and continuously perfused with oxygenated ACSF at a rate of 1-2 ml/min. Recording was done at 31 ± 1°C. The glass pipettes for patch recording had resistances of 4-8 MΩ after being filled with an internal solution containing (in mM): K-gluconate 132, HEPES 10, $MgCl_2$ 2, EGTA 5, $CaCl_2$ 0.5, ATP 4, GTP 0.5 and phosphocreatine 5, with the pH is adjusted to 7.4 ± 0.5 and the osmolarity to 285 ± 5 mOsm. The internal solution was aliquoted and stored at -20°C, and filtered before use. To perform perforated patch recordings, gramicidin, an antibiotic that forms pores in the patched membrane that are permeable to cations without disturbing the intracellular Cl^- concentration (Kyrozis and Reichling, 1995), was added to the internal solution (20 μg/ml) which was then filtered before filling the recording pipettes. In some cases, 40 mM K-gluconate in the internal saline was replaced by a molar equivalent of KCl to facilitate the detection of IPSP/Cs, as noted.

Cells were visualized under infrared Nomarski optics using the 40× water-immersion objective of an upright microscope (Olympus, BX51WI). The patch electrode was advanced toward the target cells by a micromanipulator (Sutter) and a gigaohm seal was established, typically by a small negative pressure, with the membrane ruptured by gentle suction and/or zap pulses. Signals from headstage were amplified (MultiClamp 700A, Axon Instruments), digitized (D1322, Axon), and stored on a computer hard drive for offline analysis. P-Clamp 9 software (Axon) was used for data acquisition and analysis. In some cases, dual cell recordings, in which two cells are simultaneously patched by a pair of recording electrodes, were performed to determine the variability of same cell type to identical manipulations (Zhang et al, 2012).

For control purposes, bipolar tungsten electrodes were added in some cases, with one pole positioned in a region of interest to activate specific fibers and the other in the solution nearby as a reference. For electrical stimulation, TTL signals (0.1 ms duration) were generated by a digitizer to trigger a constant current stimulator to deliver pulses over a range of 50-200 μA. For bistable cells, upstate durations were measured between the first and last spikes of membrane depolarization, whereas those of the downstate were taken as the intervening intervals of stable membrane hyperpolarization.

Pharmacological tests

In some cases, pharmacological compounds, including the AMPA receptor blocker CNQX (20 μM), the NMDA receptor blocker AP5 (30 μM), and the $GABA_a$ receptor blocker bicuculline (25 μM) or picrotoxin (100 μM) were delivered to the recording chamber through a perfusion system. For morphological identification, the recording pipettes were pre-loaded with the tracers neurobiotin or biocytin (both at 0.2-0.5%) which were then injected into the recorded cells by positive current pulses (500 pA, 500 ms on and 500 ms off) for 5-10 min at the conclusion of a session. Slices were maintained at recording conditions for another 15-20 min before being transferred to fixative (4% in paraformaldehyde 0.1 M phosphate buffer) for histology.

Fiber optics and photostimulation

TTL signals were used to trigger a LD-WL206 laser power supply connected to a MXL-473 laser (OptoEngine LLC, Utah) to generate 473 nm blue laser light pulses, which were delivered to the tissue via a 200 μm optical fiber. The tip of the optical fiber was submerged in the ACSF in the recording chamber at a tip distance of about 1.5 mm from the recording site. The power level was about 1 mW/mm^2 and the duration of the TTL signals was adjusted based on the responses (see Results).

Histology and data analysis

The histology for recovering recorded cells injected with biocytin has been described in detail elsewhere (Han et al., 2006). Briefly, whole slices were fully rinsed and incubated with the streptavidin-conjugated fluorescent dye FITC (for the Ai27 mouse) or Texas Red (for the Ai32 mouse). In some cases, slices were counterstained with a differently colored fluorescent dye (DAPI or green Nissl staining) for confocal image analysis. Data analysis was carried out using the Clampfit function of P-Clamp 9 along with Origin (OriginLab) and CorelDraw (Corel) software. Student's t-test and *post hoc* ANOVA analysis were used to determine the statistical significance, with alpha set to $P < 0.05$ unless otherwise noted.

Results

Genetic targeting of ChR2/tdTomato or ChR2/EYFP expression to PCs

The target cell types in this investigation were cerebellar cortical PCs, which were genetically labeled with a $Gad2^{cre}$ transgene, and projection cells in the DCN that are the synaptic targets of PCs. $Gad2^{cre}$ mice were interbred with Ai27 or Ai32 mice, allowing for conditional expression of ChR2-tdTomato or ChR2-EYFP, respectively (Fig. 1A). As expected, in the cerebella of $Gad2^{Cre}$/Ai27 (Fig. 1B-D) and $Gad2^{Cre}$/Ai32 mice (see below), the fluorescent reporters were expressed exclusively in GABAergic neurons, including PCs. In $Gad2^{Cre}$/Ai27 and $Gad2^{Cre}$/Ai32 mice, the tdTomato and EYFP labeling in the cerebellum was restricted to the Purkinje cell and molecular layers of the cortex (Tsubota et al, 2011), where PC somata and dendritic arbors are located, respectively, and to the DCN, where the axons of PCs terminate. An example of the tdTomato labeling in the cerebellum of a $Gad2^{Cre}$/Ai27 mouse is shown in Fig. 1B. The details of these morphological features can also be observed in confocal images, where the somata and dendrites of all examined PCs are brightly labeled (Fig. 1C). Bundles of PC axons can also readily be traced from single lobes of the cortex to the deep nuclei. In the deep nuclei, however, the target cells are not labeled, but after counterstaining with green Nissl stain were found embedded in tdTomato-positive terminals (Fig. 1D). In an optical section, these target cells showed morphological features similar to the DCN cells visualized by staining postsynaptic $GABA_a$ receptors (Garin et al, 2002).

Electrophysiological characterization of cortical PCs in $Gad2^{Cre}$/Ai27 and $Gad2^{Cre}$/Ai32 mice

While a number of studies have used optogenetic models to investigate specific functions of the cerebellum (Chaumont et al, 2013; Gutierrez et al, 2011; Sasaki et al, 2012; Tsubota et

al, 2011), there has been no detailed characterization of how individual PCs and DCN cells in such models respond to photo stimulation. The present *in vitro* study, therefore, focuses on how single PCs respond to photo stimulation and how photoactivated PC axon terminals inhibit individual cells in the DCN. In our initial characterization, the spontaneous and electrically evoked spiking of PCs in the optogenetic mice (Fig. 2A) was indistinguishable from the corresponding activity observed in controls (not shown). When focal electrical stimulation was applied to the cerebellar molecular layer to activate parallel fibers (PFs), a clear paired-pulse facilitation was observed in either current- or voltage-clamp mode (Fig. 2B), whereas similar stimulation delivered to the granular layer to activate a single climbing fiber (CF) under voltage clamp resulted in a strong paired-pulse depression (Fig. 2B). Induction of both of these forms of short-term plasticity, which are characteristic of PCs in mammals (Eccles et al, 1967; Llinas and Sugimori, 1980) and in teleost fish (Han and Bell, 2003), was consistently obtained in four animals.

Taken together, these results indicate that the electrophysiology of PCs in $Gad2^{Cre}$/Ai27 and $Gad2^{Cre}$/Ai32 mice is essentially the same as that of control mice (n=3; not shown), and that patch recording per se yields results similar to those observed in other *in vitro* preparations (Welsh et al, 2011; Zhang et al, 2012). Although the vast majority of our recordings were performed on $Gad2^{Cre}$/Ai27 mice, some were done in $Gad2^{Cre}$/Ai32 mice for control purposes. As we found no significant differences in the photoactivated responses of both PCs and DCN cells between the two mouse lines, data from both groups have been combined (see below).

We then tested the responses of PCs to photo stimulation induced by a 473 nm laser. In all cells examined, long (>100 ms) pulses generated continuous spiking at a rate of ~25 Hz (Fig. 2C; n=21). When the laser pulse length was reduced to 40 ms and given in a train, single spikes followed individual pulses up to a rate at 25-30 Hz (Fig. 2D; n=10). In comparison, an injection of inward current generated spiking at about 50 Hz (Fig. 2A). When the duration of the laser pulse was shortened further, a single stimulation as brief as 0.5-1 ms could still reliably cause these cells to depolarize and fire spikes. As shown in Fig. 2E, a dually-recorded pair of PCs under current-clamp conditions was depolarized more than 10 mV by a 1 ms light pulse, leading to the generation of a single spike in one cell and a short burst of spikes in the other. Similar depolarization and spiking in response to photo stimulation were observed in 21 PCs in both single and dual-cell recordings.

To further quantify responses to ChR2-gated current in PCs and for purposes of comparison, dual-cell recordings of paired PCs were also performed under voltage c l amp while laser pulses of variable duration were applied. It was found that a *sti*mulation a*s* brief as 0.5 ms could reliably induce an inward current of ~100 pA, while a 1 ms pulse induced a robust response of more than 400 pA that persisted for over 50 ms in both cells (Fig. 2F). The amplitude of the inward current increased proportionally with the duration of the laser pulse, reaching a maximum for 10 ms of stimulation. Further increases in pulse duration generated a plateau current that returned to baseline in about 150 ms (Fig. 2F).

Photostimulation of $Gad2^{Cre}$/Ai27 and $Gad2^{Cre}$/Ai32 mouse PCs in voltage-clamp mode induced an inward current that typically consisted of a rapidly inactivating transient and a

long-lasting steady state response at an average > 800 pA. To verify that this response to photostimulation was similar for both mouse lines, 37 PCs were taken from the Ai27 mice and 10 from the Ai32 mice. The amplitudes of steady state inward currents from these two groups of cells were 905 ± 95pA (mean ± SEM) and 917 ± 125 pA (mean ± SEM), respectively; a statistically insignificant difference ($P > 0.05$). Hence the ChR2 similarly expressed in the PCs of $Gad2^{Cre}$/Ai27(32) and $Gad2^{Cre}$/Ai32 mice is sufficiently expressed to enable these cells to be robustly activated by photostimulation in slice preparations. Pooled data from all the recorded cells (910 ± 119 pA, mean ± SEM, n=47) is summarized in Fig. 2G.

In additional recordings, our unpublished date indicate that other cortical GABAergic cells, such as stellate cells, basket cells and Golgi cells, also respond to photo stimulation, although with much more variation than we observed in PCs In stellate and basket cells, for example, photo stimulation induced a minimal depolarization that rarely reached the threshold for spiking, while the spiking behavior of Golgi cells was significantly altered. Discussion of these results is beyond the scope of this report.

Morphological identification of cerebellar cortical PCs

To ensure morphological identification of the cells recorded, slices containing cells filled with biocytin or neurobiotin were visualized using fluorescent markers (Han et al, 2006), with those expressing tdTomato (Ai27) labeled with green fluorescent streptavidin and those expressing EYFP (Ai32) labeled with red fluorescent streptavidin (Fig. 3A & B). Without exception, the physically recorded PCs were morphologically identified as such (n=29) while all PCs in the slice, including those morphologically identified, were brightly labeled with ChR2 reporters that appeared to be restricted to cell membranes, as expected (Madisen et al, 2012). As illustrated in Fig. 3C, PCs, whether labeled with red or green tracer (Fig. 3A and B), or not labeled at all, could be readily identified in a thin (1.2 μm) optical section by their fluorescent-labeled membranes (Fig. 3C). These results provide clear morphological evidence supporting our physiological recordings from PCs in this optogenetic model. The ChR2 reporters tdTomato and EYFP can be easily visualized in targeted PCs in $Gad2^{Cre}$/Ai27(32) mice, and the photoresponses in PCs are as robust and controllable as those evoked by conventional electric stimulation.

Classifications of DCN cells

The mammalian cerebellar nuclei consist of multiple subregions which include three subnuclei (from lateral to medial): the dentate nucleus, the interposed nucleus and the fastigial nucleus, where each consists of multiple types of cells (Chan-Palay, 1977; Czubayko et al, 2001) that have different connectivities and therefore, distinct functions (Baumel et al, 2009; Zhang and Raman, 2010). Histologically, each of these nuclei includes large glutamatergic and small GABAergic cells (Uusisaari and Knopfel, 2011). The present study focuses on the largest of these subregions, the laterally-located dentate nucleus, although some cells in other two nuclei and the vestibular nuclei were also recorded with similar results. We found that the spontaneous activities of these DCN cells were highly variable, ranging from a complete absence of spiking to rapid discharge ~50 Hz. In addition, some cells were bistable and showed a strong pattern of membrane oscillation in which

depolarization and burst spiking (up-state) alternated with silent phases of hyperpolarization (down-state, see below). The silent cells (with firing rates < 1 Hz; n=11, 23.4%), as well as the spontaneously firing (n=24, 51.1%) and bistable (n=12, 25.5%) ones showed a scattered distribution within each nuclear region.

Various criteria have been used to classify DCN cells. The simplest one for visualized patch recording is the soma size, which is somewhat larger for glutamatergic cells than for GABAergic cells. However, due to the overlapping morphologies of these two cell types (Uusisaari et al, 2007), classification also requires their physiological properties. As demonstrated in Fig. 4, cells with relatively large somata (>15 μm) showed strong rebound responses (Fig. 4A&B, n=31), whereas those with smaller somata (10-15 μm) had moderate rebound responses (Fig. 4C&D; n=14) to inward current injections. DCN cells with similar characteristics have previously been classified as type I and type II (Czubayko et al. 2001), and it is likely that of the cells in our two groups, the larger ones with a robust rebound phase following electrical stimulation are of type I, while the others are of type II (Fig. 4). To ensure the accuracy of these cells' classification, their responses to photo stimulation have been taken into account (see below) and their other basic properties have also been examined. It was found that the membrane input resistant, time constant and capacitance for the larger cells were 210±95 MΩ, 41±7.4 ms and 122±11.1 pF, respectively, and for smaller cells were 810±125 MΩ, 45±11.0 ms and 52±9.2 pF, measurements comparable to those previously reported (Uusisaari et al, 2007). For simplicity, we will refer to these two types of DCN cells as type I and II.

To correlate the physiological properties of DCN cells with their morphologies, patch pipettes were routinely loaded with intracellular tracer and the best-recorded cells selected for histological processing and imaging analysis. Examples of the morphologically recovered type I cells (n=14), are shown in Fig. 3 (D & E). Examples of a medium- and a small-sized cell (n=7), are also shown in Fig. 3 (F), where both cells are heavily innervated by EYFP positive-terminals. These morphological results support our physiological classification of DCN cell types, demonstrating that the ones of this optogenetic model are distinguishable by their morphology as well as by their responses to current injection. DCN cells of both subtypes were found to be innervated by ChR2-expressed PC axon terminals (Figs. 1D&3F).

Inhibition of type I DCN cells by photostimulation

We then examined the synaptic responses of type I cells to focal electrical stimulation. When brief electrical pulses (typically 50-150 μA in intensity and 0.1 ms in duration) were delivered to a nearby fiber track via a metal stimulation electrode, a biphasic response consisting of a brief EPSP followed by a longer IPSP was typically elicited under current clamp (Fig. 5A). When ionotropic glutamate receptors were pharmacologically blocked by the AMPA-type receptor antagonist CNQX (20 μM) and the NMDA-type receptor antagonist AP5 (30 μM), the evoked EPSPs disappeared but the IPSPs were enhanced, as expected (Fig. 5A; n=4).

We then examined the responses of these cells to photo stimulation using the same optical methods used for cortical PCs. As shown in Fig. 5B, strong inhibitory responses similar to

those observed following electrical stimulation occurred upon the onset of the laser pulse, but without pharmacological blockage of the glutamate receptors. Similar tests were done in 24 c ells with consistent results. When $GABA_a$ receptor antagonist bicuculline was bath applied, the photoactivated inhibition disappeared (Fig. 5B; n=5). Moreover, when the light pulse durations were reduced to as short as 1 ms, similar responses could still be consistently obtained (Fig. 5C). Additional tests showed that, as expected, the light-induced inhibition was insensitive to CNQX and AP5, but disappeared in the presence of bicuculline (Fig. 5D; n=4). By carefully adjusting the level of the laser power, unitary responses similar to spontaneously occurring current events could be elicited in three DCN cells. Spontaneous events and the light-induced responses are shown for one such cell in Fig. 5E, where a higher concentration of Cl^- in the pipette solution inverts the IPSCs. The results clearly indicate that in the $Gad2^{Cre}$/Ai27(32) mouse lines, in the absence of any pharmacological intervention, type I DCN cells can be selectively inhibited by photostimulation in a precisely controlled manner.

Responses of type II DCN cells to photostimulation

We next examined the medium- and smaller-sized DCN cells, which typically showed abbreviated rebound firing in response to hyperpolarizing current injections and hence were classified as type II, as described above (Fig. 4). Typically, laser pulses applied as before under current clamp resulted in sequences of depolarization and hyperpolarization, examples of which are shown in Fig. 6A and B (n=6). The depolarization component followed the laser pulse and was insensitive to the $GABA_a$ receptor antagonist bicuculline. The duration of the subsequent IPSP was not related to that of the laser pulse; however, this component was blocked by bicuculline and is thus similar to the IPSPs obtained in the type I DCN cells (Fig. 5). Under voltage clamp and in the presence of bicuculline, the photoactivated inward current consisted of two phases: a brief high-amplitude transient and a smaller steady-state component that persisted until the termination of the laser pulse (Fig 6C; n=4). When the level of laser power was adjusted to a near-threshold level, a 1 ms stimulation resulted in only the initial brief component. Interestingly, the amplitude of this inward current varied in a quantal fashion with the same photostimulation (Fig. 6D; n=3), suggesting a unitary response, similar to that shown for type I cells in Fig. 5E. These results indicate that similar photo stimulation as described above induces two types of responses in type II DCN cells: a direct activation mediated by ChR2 as seen in cortical PCs (Fig. 2) and a synaptic inhibition mediated by GABA release as seen in type I DCN cells (Fig. 5).

Quantitatively, light-induced inward currents in these type II cells (n=12) were in ranges of 72 ± 15.9 pA (transient component) and 23 ± 7.5 pA (steady-state component), significantly smaller than those similarly generated in PCs (Fig. 2G). Although the membrane depolarization of these photo stimulated cells was always clear, in a range of 1.5 ± 0.55 mV (n=6), the photoactivation rarely evoked spikes (Fig. 6E), even under bicuculline (n=3). These results are consistent with the notion that type II cells are likely GABAergic (Czubayko et al. 2001; Uusisaari and Knopfel, 2011).

It is important to point out that the rebound responses to electrical stimulation shown in Fig. 4 were not observed following photo stimulation of any of either type of DCN cells, even under conditions of long laser pulses at high power levels.

Photoactivation induces short-term plasticity in DCN cells

Both intrinsic and synaptic plasticity in mammalian DCN cells have been reported (Aizenman et al, 1998; Aizenman and Linden, 1999; Ouardouz and Sastry, 2000). To validate photostimulation as appropriate for investigating specific synaptic modification at the PC projection onto DCN target cells, we examined the short-term plasticity at this synapse in optogenetic mice. In these experiments, single DCN cells were patched in either voltage- or current-clamp mode and photo stimulation applied to induce synaptic inhibition. Specifically, paired 1 ms laser pulses at varying delays were generated with the laser intensity set to a level that induced a synaptic response that was about half maximal. The paired inhibitory responses were recorded from cells of both types I and II, after which the IPSCs or IPSPs were measured and paired-pulse ratios calculated for each pair of stimulations (Fig. 7A, B & D), as we have done in other preparations (Zhang and Han, 1997). As shown in Fig. 7A, a brief laser pulse reliably induced IPSCs at a constant delay (2.9±0.6 ms, n=8) and with fast kinetics (τ_{decay} =6.5±1.4 ms, n=8). Pooling these results together with the others obtained under voltage clamp, the ratio of paired IPSC amplitudes was plotted as function of the corresponding paired-pulse intervals (Fig. 7C; n=9; type I 7 cells and type II 2 cells). The same analysis was carried out with the set of results recorded under current-clamp conditions (Fig. 7D), yielding a similar relationship between synaptic responses and paired-pulse intervals (Fig. 7E; n=7, all type I cells). These summary plots almost completely reproduce the results induced by electrical stimulation under pharmacological isolation in rats reported in other studies (Caillard et al, 2000; Pedroarena and Schwarz, 2003), further supporting use of optogenetic mice in investigating the specific dynamics and plasticity of the PC-DCN cell synapse.

Modulation of DCN cell spiking by PC inhibition

We next examined how photoactivated inhibition affects the electrical activity of individual DCN cells. For these tests, cells that fired spontaneously were selected first and stimulated with 1 ms laser pulses at various frequencies. It was found that a single brief (1 ms) laser pulse could consistently shut down the spontaneous firing of a DCN cell for ~50 ms (Fig. 8A; n=12, all type I cells). If such laser pulses were delivered in short bursts to a tonically firing cell (10 Hz for 1 s), its spiking pattern could be transformed from continuous firing to a bistable progression of active and silent phases, as has been seen in other systems (Berndt et al, 2009), which persisted for the duration of the photostimulation (Fig. 8B; n=7, all type I cells).

We then selected cells undergoing spontaneous bistable firing to determine how this pattern can be modulated by both electrical currents and photostimulation. Although we found two type II cells showing spontaneous bistable firing, the following characterizations were focused on type I cells only. An example of a spontaneous bistable cell is shown in Fig. 8C, with its membrane potential switching up and down irregularly in the absence of any manipulations. In another such cell, the membrane potential reversed after longer durations

(~20 s in both the up and down states), while a brief depolarizing current pulse (25 pA for 100 ms) injected through the recording electrode reliably transitioned bursting from its silent down-state to an active upstate. Interestingly, a brief hyperpolarizing current pulse (-100 pA for 100 ms) induced similar state transitions in the same cell (Fig. 8D; n=4), as has been reported for PCs (Rokni et al, 2009). It is likely that such inward current pulse-induced state transitions were due to rebound effects (Fig. 4).

We then examined the effects of photoactivated synaptic inhibition on the firing activities of bistable cells. We first delivered single brief laser pulses (triggered by 1 ms TTL signals, as before) when a cell fired spontaneously in a bistable fashion. It was found that such photostimulation did not induce clear changes in membrane electrical activity during the down-state (not shown), but in the up-state reliably caused state transitions (n=6). Fig. 8E shows that in a pair of dual-recorded DCN cells, brief laser pulses consistently induced IPSPs (~10 mV) in the tonically firing cell of the pair while reliably switching the bistable cell from its on-state to a down-state. It is possible that this photostimulation did not induce state transitions during the down-state due to its failure to generate the rebound responses seen earlier with electrical stimulation (Fig. 4).

Next, brief laser pulses were continuously applied to mimic the tonic inhibition of PCs on bistable cells. As shown in Fig. 9A, one such cell given continuous short bursts of photostimulation (3 pulses at 20 Hz, delivered every 2 s) fired in a bistable pattern of fixed-length bursts. Upon termination of the stimulation, however, the burst durations became irregular and significantly lengthened. The regularity of this bistable pattern could be switched back and forth by turning on and off the laser pulses (not shown). The durations of the down-states of the membrane potential remained similar with (3.3 ± 0.6 s) or without (3.1 ± 0.3 s) the light-induced inhibitory inputs. However, when the tonic photostimulation was turned off, the durations of the up-states of burst firing became irregular, and significantly lengthened from 6.93.4±1.6 s to 11.4 ± 3.3 s ($P<0.01$). Measurements from 7 such bistable cells (all type I) are summarized in Fig. 9B.

Interestingly, the same photo stimulation induced IPSPs during the up-state, but “EPSPs” during the down-state (Fig. 9A, right panel). The perforated patch recordings shown in Fig. 9C demonstrate that this inversion of photostimulation-induced inhibition in bistable cells is due to the membrane potential's crossing the Cl^- equilibrium potential (E_{Cl}) during the switching between states. As illustrated in Fig. 9A (right panel), membrane potentials were ~-46 mV and ~-65 mV during the up- and down-states, respectively, while the measured E_{Cl} from 3 cells was between -58 and -62 mV (Fig. 9D).

These results indicate that inhibition from cortical PCs can bidirectionally modulate spiking behaviors of DCN cells via inhibition, shunting and excitation, and that this modulation may play an important role in maintaining DCN cell firing adaptation.

Discussion

Recently reported mouse lines allow the Cre-induced expression of optogenetic channels, potentially in any neuron that can be defined by a specific pattern of gene expression

(Madisen, et al, 2012). Here, we have used this transgenic approach to create a transgenic model, the Gad2^{Cre}/Ai27(32) mouse, of particular importance to investigations of cerebellar physiology. Gad2^{Cre}/Ai27(32) mice selectively express the light-sensitive membrane protein ChR2 in GABAergifc cells of the cerebellar system. Of the two principle cell types of interest in the present study, ChR2 expression is especially strong in all PCs, but present minimally in only a small fraction of DCN cells. These are likely to be the nuclei's GABAergic cells that project to the inferior olive. In these type II cells, as showed in Fig. 6, the direct photo responses under resting conditions rarely lead to spiking, although their synaptic responses to such photostimulation are as prominent as in all other DCN cells (compare with Fig. 5). Thus, the direct subthreshold responses to photostimulation in some DCN cells can be utilized for cell type identification.

Using this model system, we have been able to specifically target and examine the inhibition of DCN cells by cortical PCs in the mouse cerebellum. Light pulses applied to the cerebellar cortex in slice preparations from these mice reliably induced robust depolarization and spiking in all PCs examined. Similar photostimulation applied to the DCN region consistently generated strong inhibitory responses in DCN cells, confirming that such photostimulation effectively releases GABA from PC axon terminals. We have further characterized how this photoactivated, GABA-mediated inhibition modulates the spiking activities of nuclear cells and changes their firing patterns. Hence the Gad2^{Cre}/Ai27(32) mice are useful models for investigating specific synaptic interactions between cortical PCs and DCN cells.

Optogenetics has developed and evolved rapidly in neuroscience research (Deisseroth, 2014). Recently, other optogenetic methods have been utilized to investigate cerebellar functionality. These include the use of lentiviral vector transduction to examine the cerebellar control of cardiovascular function *in vivo* (Tsubota et al, 2011), as well as the creation of a transgenic mouse line to trigger the release of glutamate by Bergmann glial cells and thereby study PF-PC synapse plasticity (Sasaki et al, 2012). In another optogenetic mouse line, the use of laser light pulses to suppress PC spiking via activation of $GABA_b$ receptors altered an animal's motor learning behavior (Gutierrez et al, 2011). Most recently, an *in vivo* study has shown that photoactivation of a cluster of PCs can elicit phase-locked complex spikes in the illuminated PCs of optogenetic mice, presumably via disinhibition of a functionally closed loop in the olivo-cortico-nuclear network (Chaumont et al, 2013). While these investigations have focused on cerebellar functionality in intact animals, our study in Gad2^{Cre}/Ai27(32) mice has for the first time characterized the basic intrinsic properties of optogenetically-targeted PCs and their outputs and provides a tool for understanding the physiological mechanisms that underlie the inhibitory effects of cortical PCs on their target cells in the DCN, and thus on DCN outputs. Ultimately, this model can be applied to test how the brief photo stimulation used in our slice preparations affects these animals' motor behavior and learning.

Using retrograde labeling combined with immunohistochemistry, an elegant study has shown that a single PC can innervate multiple types of projection neurons in the DCN, including the glutamatergic cells that project to the premotor nuclei and other brain regions, as well as the GABAergic cells that project to the inferior olive (Teune et al, 1998). Our

recordings have shown that some type II DCN cells (n=12) respond to photo stimulation with a small inward current and membrane depolarization followed by a strong inhibition (Fig. 6), whereas the type I cells respond with a robust inhibition only (Fig. 5). These results suggest that at least some type II cells in this mouse model are GABAergic, whereas the type I cells are predominantly non-GABAergic. We propose that the type I and type II DCN cells recorded in our study belong to these two respective types of projection neurons. Thus, our physiological results showing that cortical PCs synaptically inhibit both glutamatergic and GABAergic nuclear cells are consistent with our morphological identification of DCN cells showing both cell types as surrounded by ChR2-positive terminals (Figs. 1D&3F).

Rebound responses have been observed in many central neurons, particularly in those of the thalamus (Grenier et al, 1998) and the inferior olive (Welsh et al, 2011), but are particularly relevant in DCN neurons because of their overwhelming inhibitory input from cortical PCs (Eccles et al, 1967; Llinás and Mühlethaler, 1988). As rebound spikes in DCN neurons are widely considered to be membrane electrical activity related to these cells' plasticity and output, and hence to cerebellar function (Bengtsson et al, 2011), they have been well characterized experimentally, predominantly in slice preparations (Aizenman and Linden, 1999; Pugh and Raman, 2006; Tadayonnejad et al, 2010). In our work, as shown in Fig. 4, robust rebound spiking consistently occurred in both types of DCN cells upon release of the membrane from an outward current injection-induced hyperpolarization. Being part of a cell's intrinsic membrane properties, such rebound responses can be reliably elicited and have been used in the classification of nuclear cell types (Czubayko et al, 2001; Uusisaari and Knöpfel, 2011). Their precise function, however, is largely speculative, and its importance has been questioned due to their weakness (Hoebeek et al, 2010) and their rarely being observed in *in vivo* preparations (Alviña et al, 2008; Freek et al, 2010; Bengtsson et al, 2011). It has been proposed that a synchronized discharge of the whole inferior olive is required for rebound responses to occur in nuclear cells, but the physiological and behavioral contexts for such a synchronization remains unclear (Bengtsson et al, 2011).

In our experiments, a brief laser pulse resulted in a complex spike-like response in cortical PCs (Fig. 2E), while similar light stimulation reliably induced IPSPs and IPSCs in all DCN cells tested (Fig. 5 & 6). As laser power levels were typically adjusted to about half of the maximal response level, it is likely that such photostimulation activated the vast majority, if not all, of PC axon terminals surrounding a recorded DCN cell. However, rebound responses resembling those typically induced in DCN neurons by current injection (Fig. 4) were not observed in any of the DCN cells stimulated optically, even when in some such cases the laser power level was significantly increased. It is unclear at this point why photo stimulation fails to induce rebound responses. A simple explanation would be that the optically evoked synaptic inhibition is insufficient to reach the threshold for T-type Ca^{2+} channel deinactivation, as would explain the rebound response generated by inward current steps. Nevertheless, our results are consistent with other published data, suggesting that the occurrence of rebound responses under physiological conditions requires further study (Alviña et al, 2008; Bengtsson et al, 2011).

Periodic membrane transitions between an up-state of depolarization with continuous spiking and a down-state that is hyperpolarized and silent are characteristic of the bistable

neurons that have been reported in many brain regions (Grenier et al, 1998; Lewis and O'Donnell, 2000; Williams et al, 2002). Such membrane bistability is probably best characterized in cerebellar PCs (Loewenstein et al, 2005; Oldfield et al, 2010; Rokni et al, 2009), where periodic spiking occurs without any clear input activation *in vivo* (Bell and Grimm, 1969) and *in vitro* (Fernandez et al, 2007; Williams et al, 2002). This suggests that bistability is largely an intrinsic membrane property, a hypothesis supported by the fact that these bistable PCs automatically switch between their up and down states across a range of membrane potentials (10-15 mV). Experimentally, brief inward or outward current pulses, or the stimulation of similarly acting synaptic inputs, have also been found effective in switching a PC's membrane state (Oldfield et al, 2010; Rokni et al, 2009; Williams et al, 2002). These data suggest that expression of membrane bistability is the result of a combination of cell's intrinsic properties and synaptic inputs. Mechanistically, a hyperpolarization-activated current (I_h) was found to serve as a “safety net” to maintain the cell membrane potential within a range necessary for generating burst firing of more than a few seconds (Williams et al, 2002). Changes in the concentration of intracellular Ca^{2+} have also been proposed to play a role in these transitions between membrane states (Rokni et al, 2006). However, the exact mechanisms determining how a neuron automatically switches its membrane potential over amplitudes of 15-20 mV remain largely unclear.

In rat DCN cells, cyclic bursting under a small constant hyperpolarization was described in type I cells and found to involve changes in intracellular Ca^{2+} levels (Czubayko et al, 2001). In our study, bistable DCN cells under resting conditions were selected by the presence of their spontaneous transitions between membrane states, as observed in both type I and type II cells. We showed that a tonically firing DCN cell could be turned into a bistable one by a burst of brief photostimulations, as is similar to what has been found for cultured hippocampal neurons (Berndt et al, 2009). This is interesting because some PCs are also bistable and as such, their firing patterns can be reversibly transmitted to their target DCN cells downstream. We further demonstrated that both brief hyperpolarizing and depolarizing current pulses can transition a cell from its down-state to an up-state in which it fires spikes (Fig. 8D). These results suggest that T-type Ca^{2+} channels probably contribute to this bistability, because DCN cells typically respond to hyperpolarizing current with a robust rebound depolarization followed by spiking (Fig. 4), and this is a cell property characteristic of the presence of these channels (Aizenman and Linden, 1999; Welsh et al, 2011). Considering that DCN cells are also known to have a strong I_h current (Aizenman and Linden, 1999; Fig. 4), the latter is also expected to contribute to DCN cell bistability, as occurs in PCs (Williams et al, 2002).

Using the dynamic clamp method, another recent study has shown that programmed current injections representing synaptic input from 40 variably synchronized PCs still elicit time-locked responses in the DCN cells at which these inputs have been modeled as converging (Person and Raman, 2011). In our study, photoactivated IPSCs in DCN cells (Fig. 7A) resemble those induced by focal electric stimulation of the nearby white matter in the presence of glutamate receptor blockers (Pedroarena and Schwarz, 2003). But our paired pulse tests also show that at ~50 Hz of photo stimulation of DCN cells, the amplitude of the second IPSC reduces to ~30% of the control value, while the second response at 30 Hz reaches ~70% (Fig. 7B&C). These results demonstrate that the short-term plasticity of the

PC-DCN synapse, which is bypassed by the dynamic clamp method, can still function as a low-pass filter in preventing synchronized high frequency signals from reaching DCN cells. The mechanisms underlying the paired-pulse depression shown here remain to be explored, and it is possible that desensitization of ChR2, as demonstrated in culture cells (Mattis et al, 2011), may contribute to such short-term plasticity.

We have further demonstrated that photoactivated synaptic inhibition can bi-directionally modulate the firing activity of DCN cells, and that tonic photo stimulation makes the timing of these transitions more regular. As illustrated in Fig. 9, photoactivated synaptic transmission in such bistable cells can be either inhibitory or excitatory, depending on the membrane status relative to the Cl^- reversal potential. Thus, our results show that synaptic inhibition from PCs plays a crucial role in modulating the firing pattern of bistable DCN cells through inhibition, shunting and excitation, as occurs in other systems (Staley and Mody, 1992; Vida et al, 2006). These results also suggest that transitions between states in a bistable cell can be governed by similar synaptic inputs, a hypothesis that is consistent with reports that both inhibitory and excitatory synaptic inputs (Loewenstein et al, 2005; Oldfield et al, 2010) as well as brief depolarizing and hyperpolarizing current steps (Rokni et al, 2009; Fig. 8D) can effectively switch the DCN membrane between its up- and down-states. A critical advantage of photostimulating DCN cells in the $Gad2^{Cre}$/Ai27(32) mouse line is that the method does not require pharmacological intervention to block inadvertent stimulation of these cells' excitatory inputs, as occurs with conventional electrical methods (Fig. 5A). It would be interesting to see how our optical stimulation of DCN cell inhibition might be combined with a similarly specific activation of these cells' mossy fiber afferents to determine how these bistable nuclear neurons integrate inhibitory signals from cortical PCs and excitatory signals from other sources to influence motor actions.

Acknowledgments

We thank Drs. Branden Nelson and Ray Daza for help with imaging analysis and Dr. AS. Khakhalin for technical assistance on perforate-patch recording. We also thank Dr. John Welsh for valuable comments on an earlier version of the manuscript. This work is supported by grants from the NSF (IOS1001767 to V.Z.H) and NIH (R01MH093667 to E.T).

References

Aizenman CD, Manis PB, Linden DJ. Polarity of long-term synaptic gain change is related to postsynaptic spike firing at a cerebellar inhibitory synapse. Neuron. 1998; 21(4):827–835. [PubMed: 9808468]

Aizenman CD, Linden DJ. Regulation of the rebound depolarization and spontaneous firing patterns of deep nuclear neurons in slices of rat cerebellum. J Neurophysiol. 1999; 82(4):1697–1709. [PubMed: 10515960]

Alviña K, Walter JT, Kohn A, Ellis-Davies G, Khodakhah K. Questioning the role of rebound firing in the cerebellum. Nat Neurosci. 2008; 11(11):1256–1258. [PubMed: 18820695]

Apps R, Garwicz M. Anatomical and physiological foundations of cerebellar information processing. Nat Rev Neurosci. 2005; 6(4):297–311. [PubMed: 15803161]

Baumel Y, Jacobson GA, Cohen D. Implications of functional anatomy on information processing in the deep cerebellar nuclei. Front Cell Neurosci. 2009; 3:14. [PubMed: 19949453]

Bell CC, Grimm RJ. Discharge properties of Purkinje cells recorded on single and double microelectrodes. J Neurophysiol. 1969; 32(6):1044–1055. [PubMed: 5347706]

Bell CC, Han VZ, Sawtell NB. Cerebellum-like structures and their implications for cerebellar function. Annu Rev Neurosci. 2008; 31:1–24. [PubMed: 18275284]

Bengtsson F, Ekerot CF, Jörntell H. *In vivo* analysis of inhibitory synaptic inputs and rebounds in deep cerebellar nuclear neurons. PLoS One. 2011; 6(4):e18822. [PubMed: 21552556]

Berndt A, Yizhar O, Gunaydin LA, Hegemann P, Deisseroth K. Bi-stable neural state switches. Nat Neurosci. 2009; 12(2):229–234. 2009. [PubMed: 19079251]

Caillard O, Moreno H, Schwaller B, Llano I, Celio MR, Marty A. Role of the calcium-binding protein paralbumin in short-term synaptic plasticity. Proc Natl Acad Sci U S A. 2000; 97(24):13372–13377. [PubMed: 11069288]

Chan-Palay, V. Cerebellar dentate nucleus Organization, Cytology, and Transmitters. Springer; New York: 1977.

Chaumont J, Guyon N, Valera AM, Dugué GP, Popa D, Marcaggi P, Gautheron V, Reibel-Foisset S, Dieudonné S, Stephan A, Barrot M, Cassel JC, Dupont JL, Doussau F, Poulain B, Selimi F, Léna C, Isope P. Clusters of cerebellar Purkinje cells control their afferent climbing fiber discharge. Proc Natl Acad Sci U S A. 2013; 110(40):16223–16228. [PubMed: 24046366]

Czubayko U, Sultan F, Thier P, Schwarz C. Two types of neurons in the rat cerebellar nuclei as distinguished by membrane potentials and intracellular fillings. J Neurophysiol. 2001; 85(5):2017–2029. [PubMed: 11353018]

Deisseroth K. Circuit dynamics of adaptive and maladaptive behaviour. Nature. 2014; 505(7483):309–17. [PubMed: 24429629]

Eccles, JC., Ito, M., Szentagothai, J. The Cerebellum as a Neuronal Machine. Heidelberg: Springer-Verlag; 1967.

Fernandez FR, Engbers JD, Turner RW. Firing dynamics of cerebellar Purkinje cells. J Neurophysiol. 2007; 98(1):278–294. [PubMed: 17493923]

Hoebeek, Freek E., Witter, Laurens, Ruigrok, Tom JH., De Zeeuw, Chris I. Differential olivo-cerebellar cortical control of rebound activity in the cerebellar nuclei. Proc Natl Acad Sci U S A. 2010; 107(18):8410–8415. [PubMed: 20395550]

Gao Z, van Beugen BJ, De Zeeuw CI. Distributed synergistic plasticity and cerebellar learning. Nat Rev Neurosci. 2012; 13(9):619–635. [PubMed: 22895474]

Garin N, Hornung JP, Escher G. Distribution of postsynaptic GABA(A) receptor aggregates in the deep cerebellar nuclei of normal and mutant mice. J Comp Neurol. 2002; 447(3):210–217. [PubMed: 11984816]

Grenier F, Timofeev I, Steriade M. Leading role of thalamic over cortical neurons during postinhibitory rebound excitation. Proc Natl Acad Sci U S A. 1998; 95(23):13929–13934. [PubMed: 9811903]

Gutierrez DV, Mark MD, Masseck O, Maejima T, Kuckelsberg D, Hyde RA, Krause M, Kruse W, Herlitze S. Optogenetic control of motor coordination by $G_{i/o}$ protein-coupled vertebrate rhodopsin in cerebellar Purkinje cells. J Biol Chem. 2011; 286(29):25848–26858. [PubMed: 21628464]

Han VZ, Bell CC. Physiology of cells in the central lobes of the mormyrid cerebellum. J Neurosci. 2003; 23(35):11147–11157. [PubMed: 14657174]

Han VZ, Meek J, Campbell HR, Bell CC. Cell morphology and circuitry in the central lobes of the mormyrid cerebellum. J Comp Neurol. 2006; 497(3):309–325. [PubMed: 16736465]

Hansel C, Linden DJ, DAngelo E. Beyond parallel fiber LTD: the diversity of synaptic and non-synaptic plasticity in the cerebellum. Nat Neurosci. 2001; 4(5):467–475. [PubMed: 11319554]

Hoebeek FE, Witter L, Ruigrok TJ, De Zeeuw CI. Differential olivo-cerebellar cortical control of rebound activity in the cerebellar nuclei. Proc Natl Acad Sci U S A. 2010; 107(18):8410–8415. [PubMed: 20395550]

Ito, M. The Cerebellum and Neural Control. New York: Raven Press; 1984.

Ito M. Cerebellar long-term depression: characterization, signal transduction, and functional roles. Phys Rev. 2001; 81(3):1143–1195.

Jacobson GA, Rokni D, Yarom Y. A model of the olivo-cerebellar system as a temporal pattern generator. Trends Neurosci. 2008; 31(12):617–625. [PubMed: 18952303]

Jaeger D. Mini-review: synaptic integration in the cerebellar nuclei--perspectives from dynamic clamp and computer simulation studies. Cerebellum. 2011; 10(4):659–666. [PubMed: 21259124]

Jörntell H, Hansel C. Synaptic memories upside down: bidirectional plasticity at cerebellar parallel fiber-Purkinje cell synapses. Neuron. 2006; 52(2):227–238. [PubMed: 17046686]

Kyrozis A, Reichling DB. Perforated-patch recording with gramicidin avoids artifactual changes in intracellular chloride concentration. J Neurosci Methods. 1995; 57(1):27–35. [PubMed: 7540702]

Leiner HC, Leiner AL, Dow RS. Cognitive and language functions of the human cerebellum. Trends Neurosci. 1993; 16(11):444–447. [PubMed: 7507614]

Lewis BL, O'Donnell P. Ventral tegmental area afferents to the prefrontal cortex maintain membrane potential 'up' states in pyramidal neurons via D(1) dopamine receptors. Cereb Cortex. 2000; 10(12):1168–1175. [PubMed: 11073866]

Llinás R, Sugimori M. Electrophysiological properties of *in vitro* Purkinje cell dendrites in mammalian cerebellar slices. J Physiol (Lond). 1980; 305:197–213. [PubMed: 7441553]

Llinás R, Mühlethaler M. Electrophysiology of guinea-pig cerebellar nuclear cells in the in vitro brain stem-cerebellar preparation. J Physiol. 1988; 404:241–258. [PubMed: 2855348]

Loewenstein Y, Mahon S, Chadderton P, Kitamura K, Sompolinsky H, Yarom Y, Hausser M. Bistability of cerebellar Purkinje cells modulated by sensory stimulation. Nat Neurosci. 2005; 8(2):202–211. [PubMed: 15665875]

Madisen L, Mao T, Koch H, Zhuo JM, Berenyi A, Fujisawa S, Hsu YW, Garcia AJ 3rd, Gu X, Zanella S, Kidney J, Gu H, Mao Y, Hooks BM, Boyden ES, Buzsáki G, Ramirez JM, Jones AR, Svoboda K, Han X, Turner EE, Zeng H. A toolbox of Cre-dependent optogenetic transgenic mice for light-induced activation and silencing. Nat Neurosci. 2012; 15(5):793–802. [PubMed: 22446880]

Mattis J, Tye KM, Ferenczi EA, Ramakrishnan C, O'Shea DJ, Prakash R, Gunaydin LA, Hyun M, Fenno LE, Gradinaru V, Yizhar O, Deisseroth K. Principles for applying optogenetic tools derived from direct comparative analysis of microbial opsins. Nat Methods. 2011; 9(2):159–172. [PubMed: 22179551]

Mauk MD, Donegan NH. A model of Pavlovian eyelid conditioning based on the synaptic organization of the cerebellum. Learn Mem. 1997; 4(1):130–158. [PubMed: 10456059]

McDevitt CJ, Ebner TJ, Bloedel JR. Relationships between simultaneously recorded Purkinje cells and nuclear neurons. Brain Res. 1987; 425(1):1–13. [PubMed: 3427412]

Nagel G, Ollig D, Fuhrmann M, Kateriya S, Musti AM, Bamberg E, Hegemann P. Channelrhodopsin-1: a light-gated proton channel in green algae. Science. 2002; 296(5577):2395–2398. [PubMed: 12089443]

Ohyama T, Nores WL, Medina JF, Riusech FA, Mauk MD. Learning-induced plasticity in deep cerebellar nucleus. J Neurosci. 2006; 26(49):12656–12663. [PubMed: 17151268]

Oldfield CS, Marty A, Stell BM. Interneurons of the cerebellar cortex toggle Purkinje cells between up and down states. Proc Natl Acad Sci U S A. 2010; 107(29):13153–13158. [PubMed: 20615960]

Ouardouz M, Sastry BR. Mechanisms underlying LTP of inhibitory synaptic transmission in the deep cerebellar nuclei. J Neurophysiol. 2000; 84(3):1414–1421. [PubMed: 10980014]

Palkovits M, Mezey E, Hamori J, Szentagothai J. Quantitative histological analysis of the cerebellar nuclei in the cat. I. Numerical data on cells and synapses. Exp Brain Res. 1977; 28(1-2):189–209. [PubMed: 881003]

Pedroarena CM, Schwarz C. Efficacy and short-term plasticity at GABAergic synapses between Purkinje and cerebellar nuclei neurons. J Neurophysiol. 2003; 89(2):704–715. [PubMed: 12574448]

Person AL, Raman IM. Purkinje neuron synchrony elicits time-locked spiking in the cerebellar nuclei. Nature. 2011; 481(7382):502–505. [PubMed: 22198670]

Pugh JR, Raman IM. Potentiation of mossy fiber EPSCs in the cerebellar nuclei by NMDA receptor activation followed by postinhibitory rebound current. Neuron. 2006; 51(1):113–123. [PubMed: 16815336]

Raymond JL, Lisberger SG, Mauk MD. The cerebellum: a neuronal learning machine? Science. 1996; 272(5265):1126–1131. [PubMed: 8638157]

Rokni D, Tal Z, Byk H, Yarom Y. Regularity, variability and bi-stability in the activity of cerebellar Purkinje cells. Front Cell Neurosci. 2009; 3:12. [PubMed: 19915724]

Sasaki T, Beppu K, Tanaka KF, Fukazawa Y, Shigemoto R, Matsui K. Application of an optogenetic byway for perturbing neuronal activity via glial photo stimulation. Proc Natl Acad Sci U S A. 2012; 109(50):20720–20725. [PubMed: 23185019]

Schonewille M, Khosrovani S, Winkelman BH, Hoebeek FE, De Jeu MT, Larsen IM, Van der Burg J, Schmolesky MT, Frens MA, De Zeeuw CI. Purkinje cells in awake behaving animals operate at the upstate membrane potential. Nat Neurosci. 2006; 9(4):459–461. [PubMed: 16568098]

Shutoh F, Ohki M, Kitazawa H, Itohara S, Nagao S. Memory trace of motor learning shifts transsynaptically from cerebellar cortex to nuclei for consolidation. Neuroscience. 2006; 139(2): 767–777. [PubMed: 16458438]

Staley KJ, Mody I. Shunting of excitatory input to dentate gyrus granule cells by a depolarizing GABAA receptor-mediated postsynaptic conductance. J Neurophysiol. 1992; 68(1):197–212. [PubMed: 1381418]

Stoodley CJ, Valera EM, Schmahmann JD. Functional topography of the cerebellum for motor and cognitive tasks: an fMRI study. Neuroimage. 2012; 59(2):1560–1570. [PubMed: 21907811]

Sugihara I. Compartmentalization of the deep cerebellar nuclei based on afferent projections and aldolase C expression. Cerebellum. 2011; 10(3):449–463. [PubMed: 20981512]

Tadayonnejad R, Anderson D, Molineux ML, Mehaffey WH, Jayasuriya K, Turner RW. Rebound discharge in deep cerebellar nuclear neurons *in vitro*. Cerebellum. 2010; 9(3):352–374. [PubMed: 20396983]

Taniguchi H, He M, Wu P, Kim S, Paik R, Sugino K, Kvitsiani D, Fu Y, Lu J, Lin Y, Miyoshi G, Shima Y, Fishell G, Nelson SB, Huang ZJ. A resource of Cre driver lines for genetic targeting of GABAergic neurons in cerebral cortex. 2011; 71(6):995–1013.

Teune TM, van der Burg J, de Zeeuw CI, Voogd J, Ruigrok TJ. Single Purkinje cell can innervate multiple classes of projection neurons in the cerebellar nuclei of the rat: a light microscopic and ultrastructural triple-tracer study in the rat. J Comp Neurol. 1998; 392(2):164–178. [PubMed: 9512267]

Teune TM, van der Burg J, van der Moer J, Voogd J, Ruigrok TJ. Topography of cerebellar nuclear projections to the brain stem in the rat. Prog Brain Res. 2000; 124:141–172. [PubMed: 10943123]

Tsubota T, Ohashi Y, Tamura K, Sato A, Miyashita Y. Optogenetic manipulation of cerebellar Purkinje Cell Activity *in vivo*. PloS One. 2011; 6(8):e22400. [PubMed: 21850224]

Tye KM, Deisseroth K. Optogenetic investigation of neural circuits underlying brain disease in animal models. Nat Rev Neurosci. 2012; 13(4):251–266. [PubMed: 22430017]

Uusisaari M, De Schutter E. The mysterious microcircuitry of the cerebellar nuclei. J Physiol. 2011; 589(Pt. 14):3441–3457. [PubMed: 21521761]

Uusisaari M, Knöpfel T. Functional classification of neurons in the mouse lateral cerebellar nuclei. Cerebellum. 2011; 10(4):637–646. [PubMed: 21116763]

Uusisaari M, Obata K, Knöpfel T. Morphological and electrophysiological properties of GABAergic and non-GABAergic cells in the deep cerebellar nuclei. J Neurophysiol. 2007; 97(1):901–11. [PubMed: 17093116]

Vida I, Bartos M, Jonas P. Shunting inhibition improves robustness of gamma oscillations in hippocampal interneuron networks by homogenizing firing rates. Neuron. 2006; 49(1):107–117. [PubMed: 16387643]

Voogd J, Glickstein M. The anatomy of the cerebellum. Trends Neurosci. 1998; 21(9):370–375. [PubMed: 9735944]

Welsh JP, Lang EJ, Sugihara I, Llinás R. Dynamic organization of motor control within the olivocerebellar system. Nature. 1995; 374(6521):453–457. [PubMed: 7700354]

Welsh JP, Han VZ, Rossi DJ, Mohr C, Odagiri M, Daunais JB, Grant KA. Bidirectional plasticity in the primate inferior olive induced by chronic ethanol intoxication and sustained abstinence. Proc Natl Acad Sci U S A. 2011; 108(25):10314–10319. [PubMed: 21642533]

Williams SR, Christensen SR, Stuart GJ, Häusser M. Membrane potential bistability is controlled by the hyperpolarization-activated current I(H) in rat cerebellar Purkinje neurons in vitro. J Physiol. 2002; 539(Pt. 2):469–583. [PubMed: 11882679]

Zhang N, Raman IM. Synaptic inhibition, excitation, and plasticity in neurons of the cerebellar nuclei. Cerebellum. 2010; 9(1):56–66. [PubMed: 19847585]

Zhang Y, Han VZ. Physiology of morphologically identified cells in the posterior caudal lobe of the mormyrid cerebellum. J Neurophysiol. 1997; 98(3):1297–1308.

Zhang Y, Magnus G, Han VZ. Synaptic dynamics and long-term plasticity at synapses of Purkinje cells onto neighboring Purkinje cells: a dual cell recording study. Neuroscience. 2012; 225:199–212. [PubMed: 22906478]

Research Highlights

Photoactivation of Purkinje cells;

Synaptic inhibition of nuclear cells by Purkinje cells;

Modulations of firing patterns of nuclear cells by Purkinje cell inhibition;

Optogenetic mouse model.

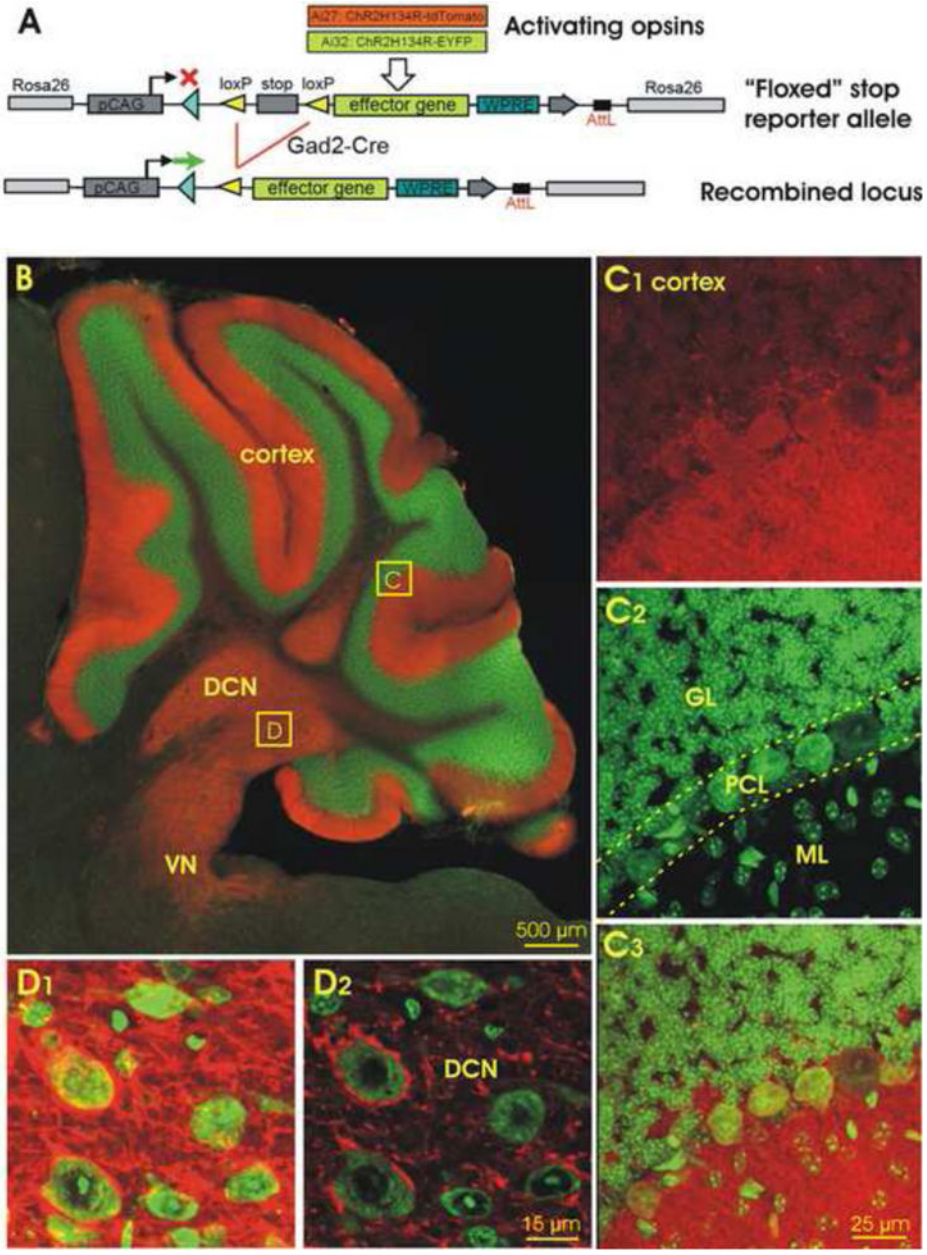

Fig. 1. Generation and characterization of Gad2^{Cre}/Ai27 and Gad2^{Cre}/Ai32 mice expressing tdTomato- or EYFP-ChR2 in GABAergic cerebellar neurons

A. Schematic for the activation of an inducible ChR2-tdTomato or ChR2-EYFP gene targeted to the Rosa26 locus using Gad2^{Cre}. **B.** Image of the Gad2^{Cre}/Ai27 mouse cerebellum in a parasagittal plane, showing tdTomato (red) counterstained with Nissl fluorescence (green). DCN, deep cerebellar nuclei; VN, vestibular nuclei. **C.** Confocal images of boxed area C of the cerebellar cortex in B, showing strong ChR2-tdTomato fluorescence in both somas and dendrites of PCs (C_1), Nissl staining with green fluorescent dye (C_2), and their overlay (C_3). GL, granular layer; ML, molecular layer; PCL, Purkinje cell layer. **D.** Confocal image of a DCN region in B (boxed area D) in a Z-stack (10.5 μm,

D_1) and in a single optical section (0.5 μm, D_2), showing that cells are heavily innervated by ChR2-positive fibers. Scale bar: 500 μm in B, 25 μm in C, and 15 μm in D.

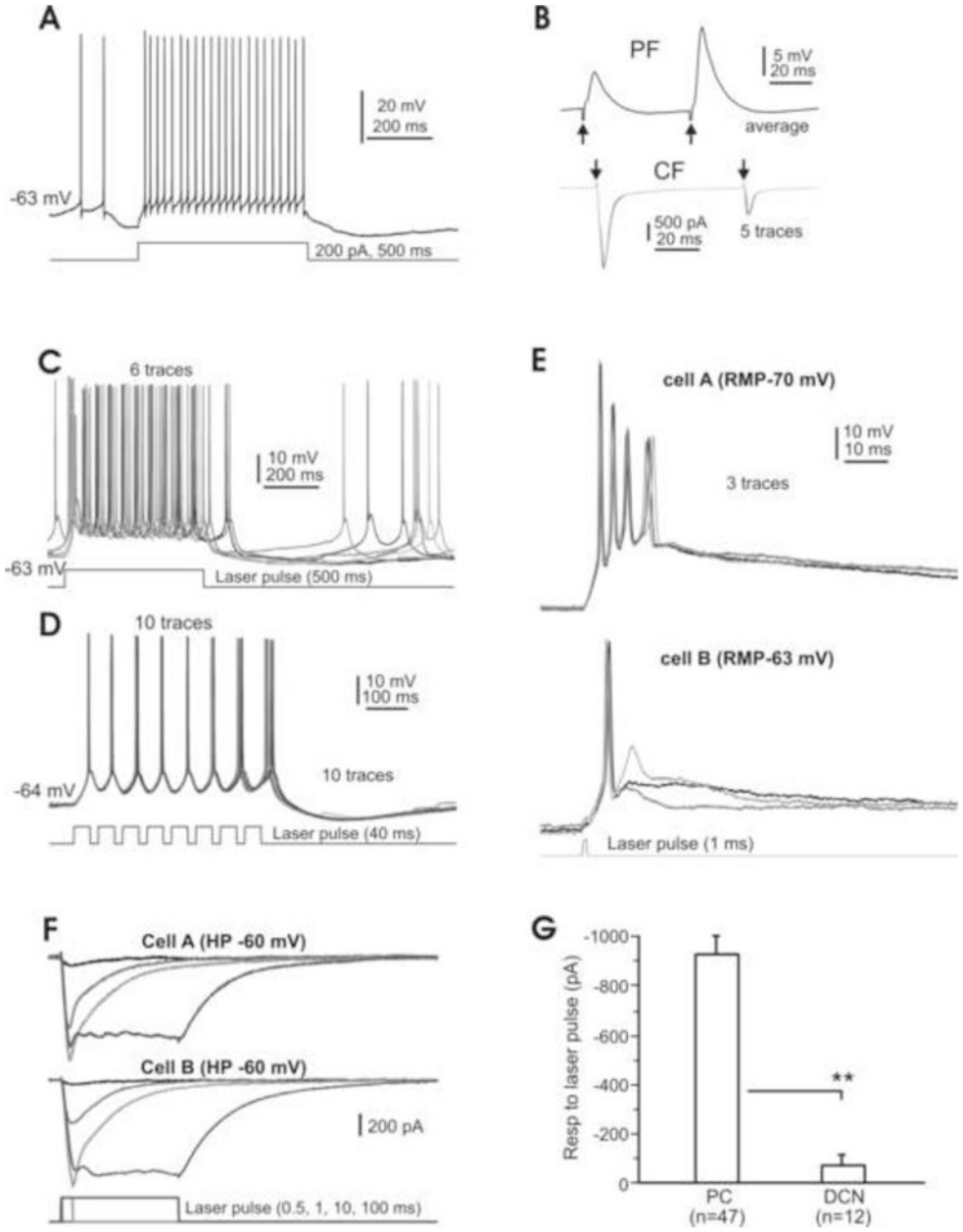

Fig. 2. Physiology of Purkinje cells in Gad2^{Cre}/Ai27(32) mice

A. Typical spiking of a Purkinje cell, spontaneously and in response to an inward current step. **B.** Responses of the same cell shown in A to parallel fiber (PF, top) and climbing fiber (CF, bottom) activation. Note the respective paired-pulse facilitation and depression of the PF and CF responses. **C.** Evoked burst spiking at ~25 Hz elicited by a 500 ms laser pulse, followed by spontaneous spiking. **D.** Shorter (40 ms) laser pulses evoke spiking at 25 Hz. **E.** Dual recordings of a pair of PCs under current-clamp conditions. A single brief (1 ms) laser pulse reliably elicits a large depolarization and spikes in both cells. Note the complex spike-like responses in cell A. **F.** Dual recordings of a pair of PCs in voltage-clamp mode, showing that laser pulses at variable durations evoke robust inward currents consisting of phasic and plateau components in both cells. **G.** Plateau current responses of different cell types to

longer laser pulses (≥50 ms). RMP, resting membrane potential; PC, Purkinje cells; DCN, (small- and medium-sized) deep cerebellar nuclear cells. **, P<0.01. Note that here and in the following figures, single or average traces are shown unless otherwise specified.

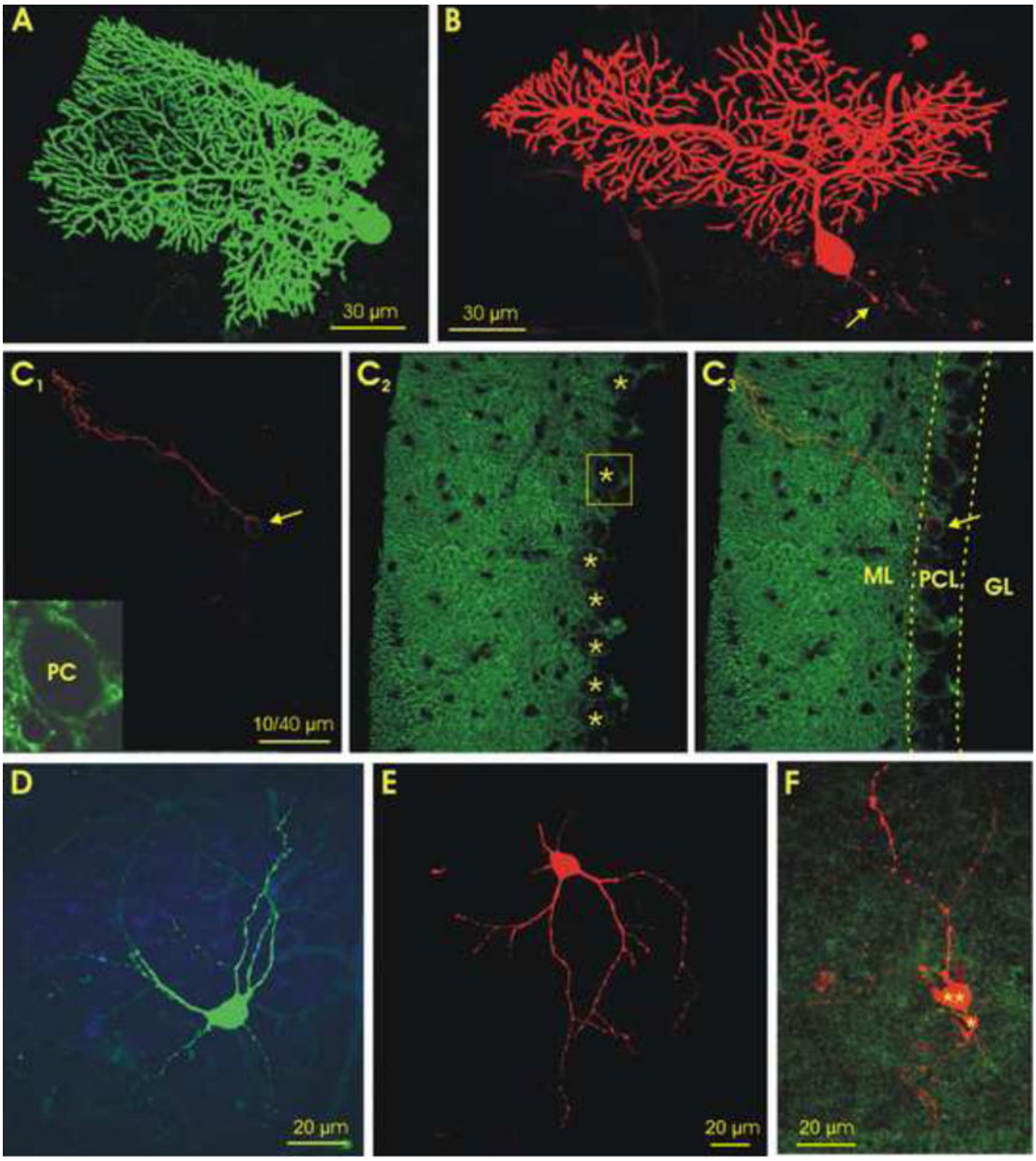

Fig. 3. Morphology of cerebellar cortical and deep nuclear cells filled with intracellular tracers following their physiological characterization

A&B. Confocal images of two Purkinje cells in parasagittal slices, labeled with green fluorescent dye in a $Gad2^{Cre}$/Ai27 mouse (with a tdTomato reporter) (A), and with red fluorescent dye in a $Gad2^{Cre}$/Ai32 mouse (with an EYFP reporter) (B). Note that the axon of the cell in B was cut during slicing (arrow). **C.** Images of a 1.2 μm thick optical section of a $Gad2^{Cre}$/Ai32 mouse cerebellum. **C_1**. A biocytin labeled PC (red, arrow). **C_2**. EYFP-labeled GABAergic cells, where the PC dendrites are heavily labeled in the molecular layer while the PC somas in the Purkinje cell layer are primarily labeled in their plasma membranes (asterisks). **C_3**. Overlay of C_1 and C_2. Inset in C_1 is enlarged boxed area of C_2, showing a PC soma with clear EYFP-labeled membrane. **D&E**. Confocal images of two large DCN

cells labeled with green and red fluorescent dye from GAD2^{Cre}/Ai27 (D) and GAD2^{Cre}/Ai32 (E) mice, respectively. **F.** A confocal stack image of labeled, physiologically-characterized small- (asterisks) and medium-sized (double asterisks) DCN cells from a Gad2^{Cre}/Ai32 mouse, showing both labeled cells surrounded by green GAD2 positive terminals. GL, granular layer; ML, molecular layer; PCL, Purkinje cell layer; PC, Purkinje cell. Scale bars: 30 μm in A and B, 40 μm in C, 20 μm in D-F.

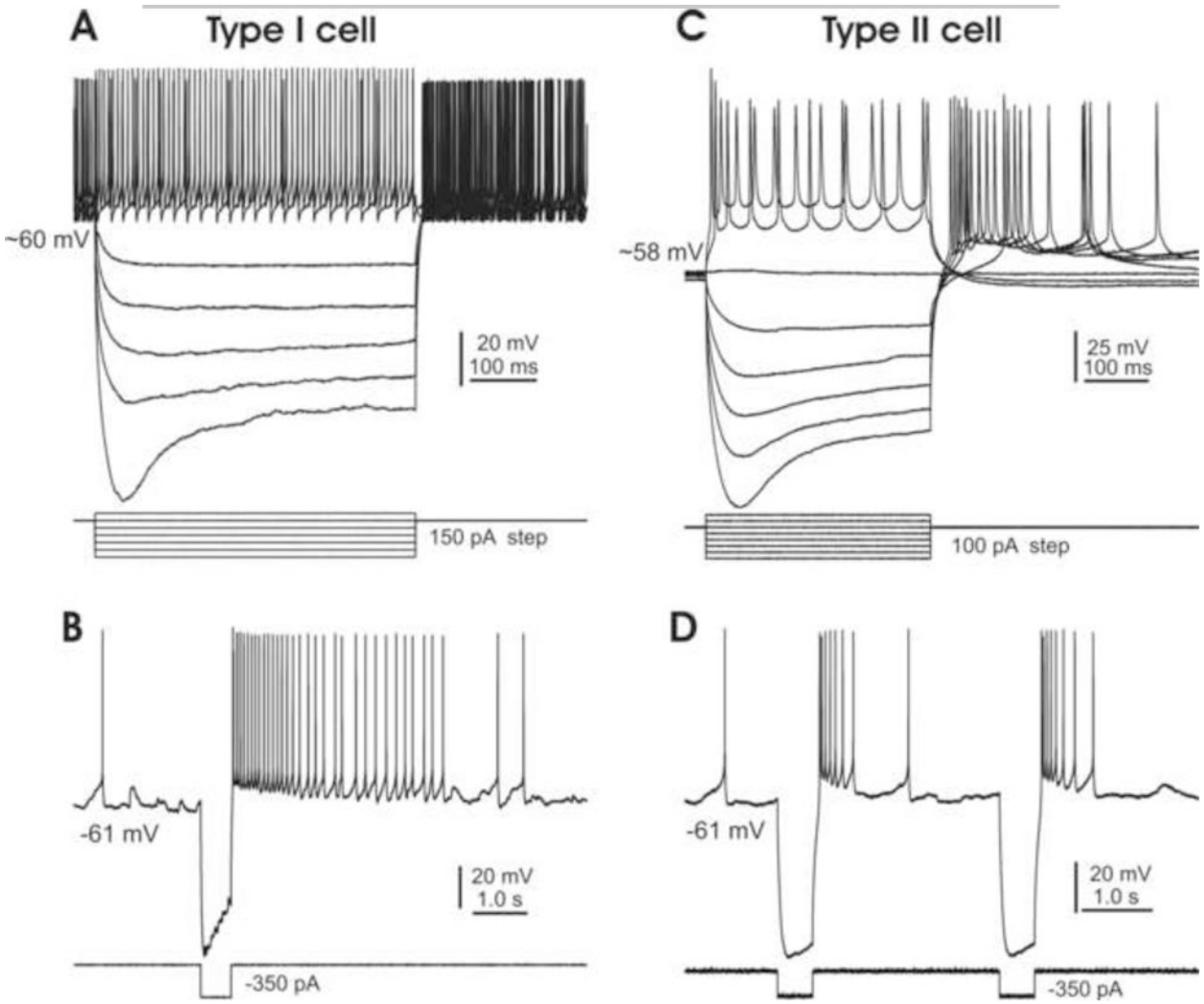

Fig. 4. Physiology of representative DCN cells

A. A type I cell, showing a high level of spontaneous firing, a large “sag” and robust rebound firing in response to hyperpolarizing current steps. **B. A** single hyperpolarizing current step (350 pA) induces robust rebound responses in a type I cell under resting conditions. **C.** A type II cell also shows a large “sag” but only moderate rebound firing in response to similar current steps. **D.** A single hyperpolarizing current step (350 pA) induces moderate rebound responses in a type II cell under resting conditions. Note that responses of both types of cells to hyperpolarizing inward current injections are similar to those reported by Czubayko et al, 2001.

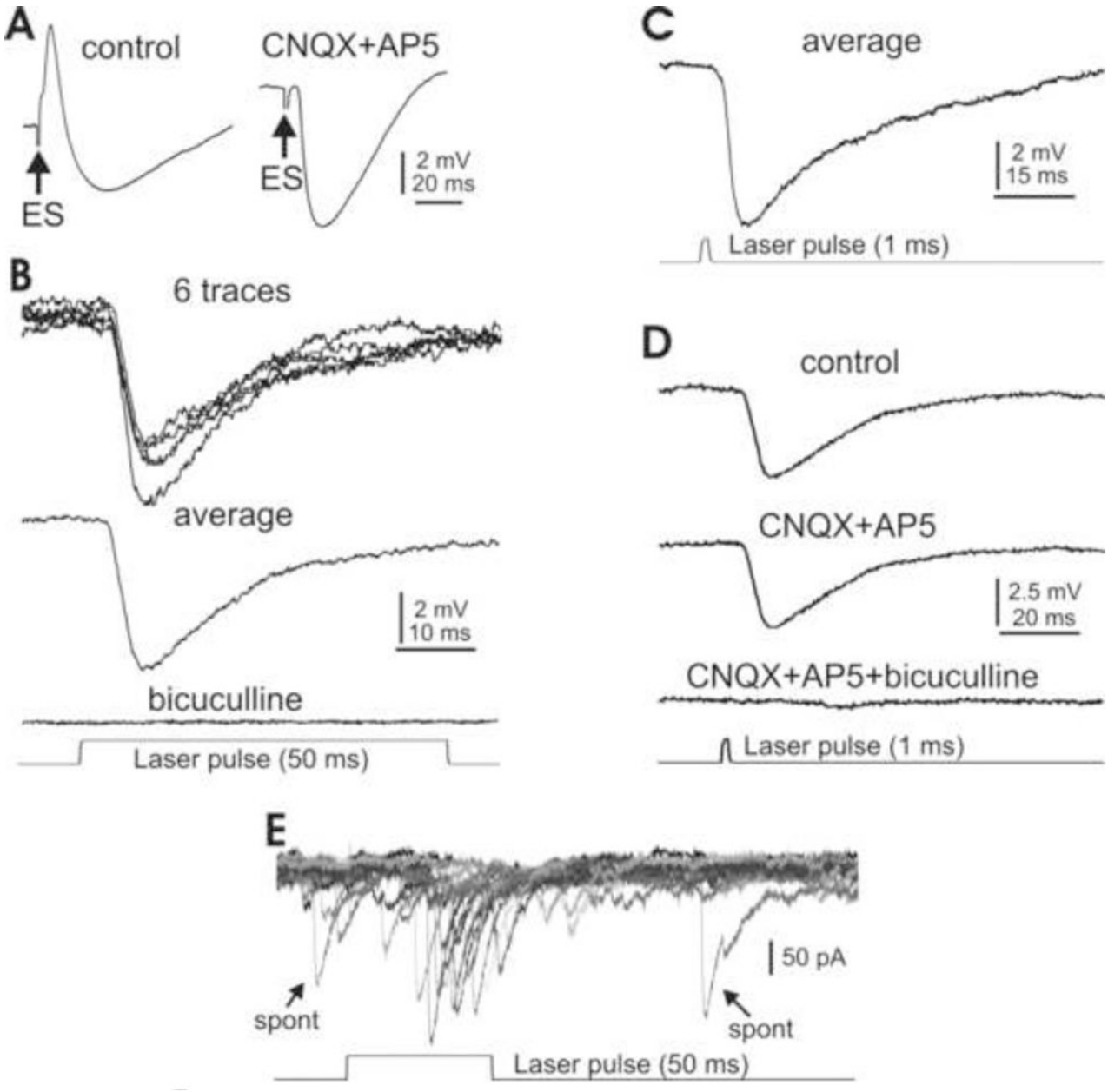

Fig. 5. Synaptic inhibition of type I DCN cells by electrical and optical stimulation

A. Typical IPSP evoked by focal electrical stimulation in a large DCN cell pharmacologically isolated by bath application of ionotropic glutamate receptor antagonists CNQX and AP5. **B.** A 50 ms laser pulse evokes similar inhibitory responses in another DCN cell, without any receptor blockers. The response is eliminated when the $GABA_a$ receptor blocker bicuculline is bath applied. **C.** A 1 ms laser pulse reliably evokes DCN cell inhibition similar to that seen in response to the 50 ms stimulation in the presence of CNQX and AP5 (A, right panel and B). **D.** The photostimulation-evoked IPSP is insensitive to ionotropic glutamate receptor antagonists CNQX and AP5, but disappears in the presence of bicuculline. **E.** A 50 ms laser pulse at threshold level evokes unitary inward current events

similar to spontaneous IPSCs (arrows). Note that the IPSCs are inverted due to a high Cl^- concentration in the internal solution.

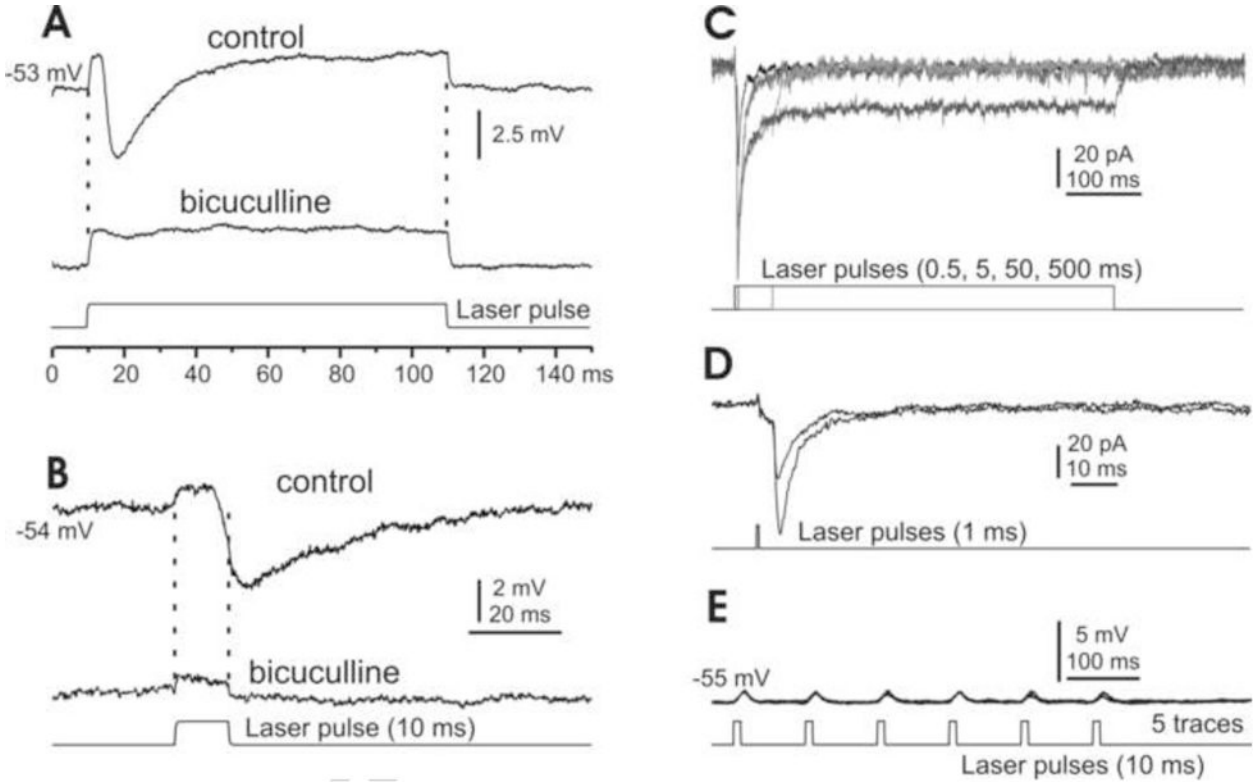

Fig. 6. Responses of type II DCN cells to photostimulation

A&B. Under current-clamp conditions, long (A) and short (B) laser pulses induce depolarization mixed with IPSPs in small DCN cells, where the IPSPs, but not the depolarizations, are sensitive to the $GABA_a$ receptor blocker bicuculline. **C.** Under voltage clamp and in the presence of bicuculline, photostimulation of varying durations induces inward currents that typically include phasic and plateau components. **D.** A brief laser pulse at constant intensity induces current responses that vary in size by discrete steps, suggesting a unitary response at this synapse. **E.** A typical type II DCN cell, showing that 1 ms laser pulses induce depolarization, but rarely spiking.

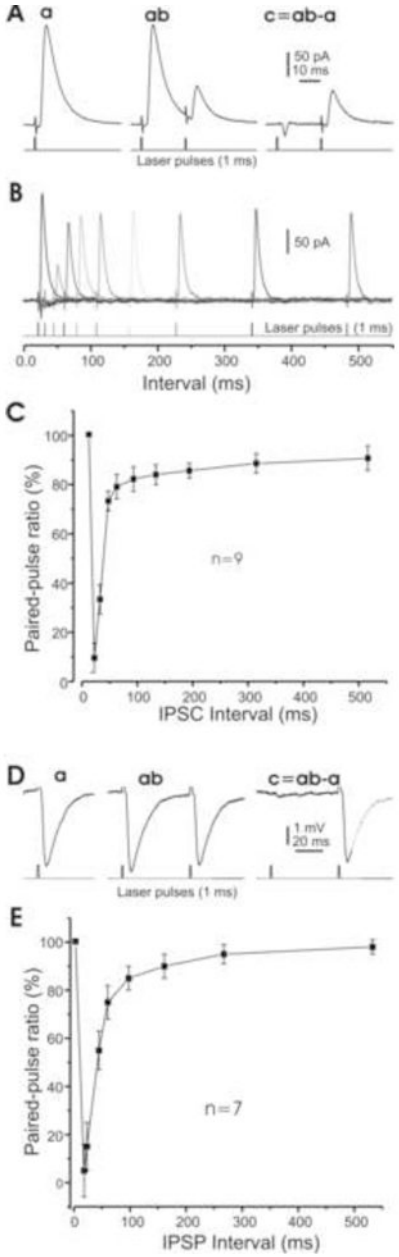

Fig. 7. Short-term plasticity of synaptic inhibition in DCN cells

A. Examples of averaged IPSCs induced by brief (1 ms) laser pulses. The left panel (a) is subtracted from the middle panel (ab) to give the right panel (c). **B.** Examples of IPSCs in one cell in response to paired laser pulses at varying interpulse intervals. **C.** Pooled data of 9 cells, showing the ratio of paired-pulse inhibition amplitudes as a function of paired laser-pulse intervals. Note that the response to the second pulse disappears, but then recovers to ~30% and ~80% of the amplitude of the first pulse for interpulse intervals of ~10, ~25 and ~70 ms, respectively. **D.** Examples of averaged IPSPs induced by photo stimulation similar to A. **E.** Pooled data of 7 cells, showing that the inhibition is largely recovered for an interpulse interval of ~100 ms. Note that some cells were recorded under both voltage- and current-clamp configurations, and are therefore included in both groups.

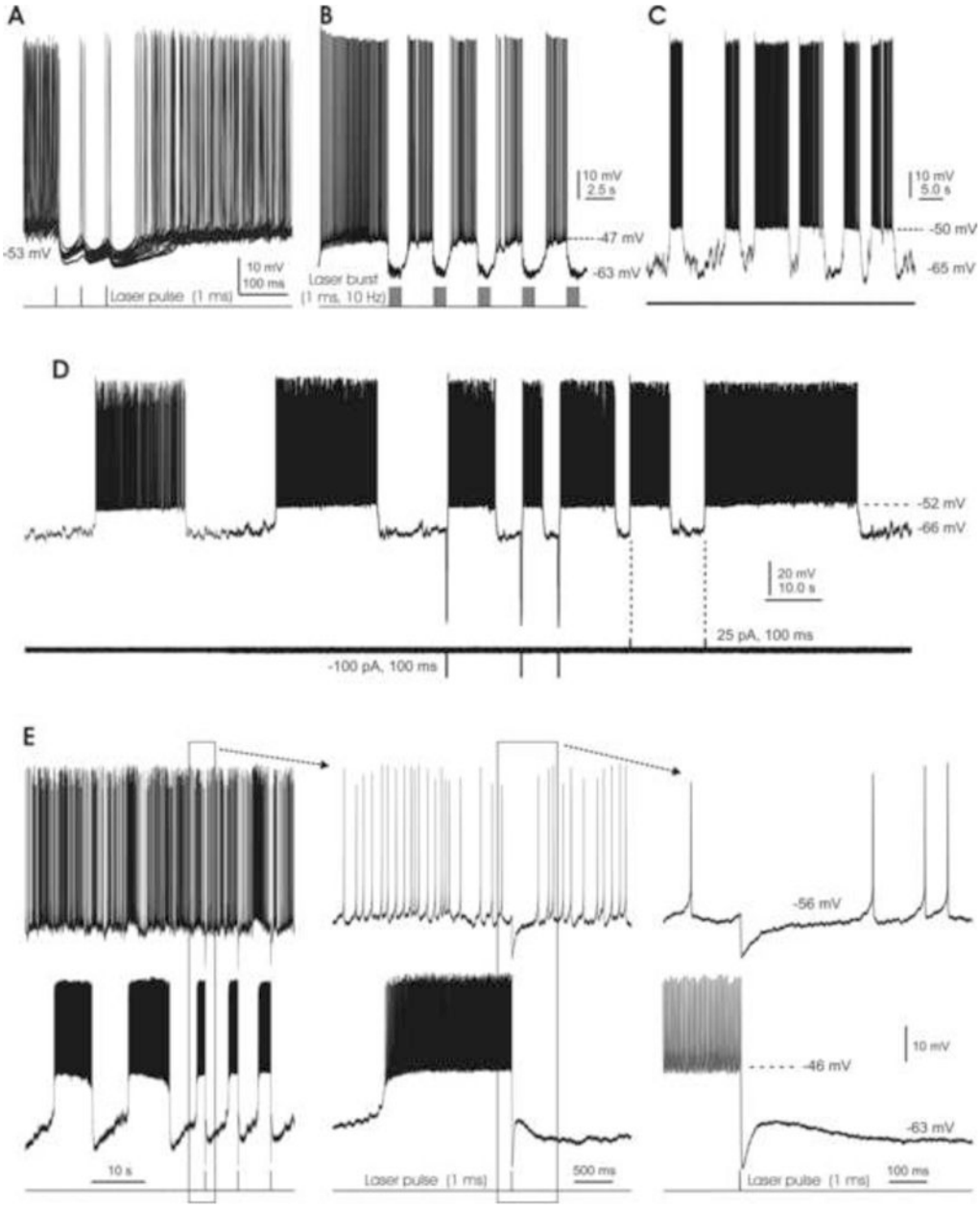

Fig. 8. Bistability of DCN cell membrane potential

A. Brief (1 ms) laser pulses consistently induce robust IPSPs which pause spontaneous firing for ~50 ms. **B.** Bursts of 1 ms laser pulses (10 Hz for 1 s) replace the cell's spontaneous tonic spiking with a bistable firing pattern. **C.** A spontaneously bistable cell under resting conditions, without any manipulations. **D.** Another spontaneously bistable cell is switched from its down-state to its up-state by either brief hyperpolarizing or depolarizing current pulses. Note the longer and more regular burst firing that occurs in the absence of current injections. **E**. A pair of DCN cells, with spontaneously tonic (top) and bistable (bottom) firing patterns. The middle and right panels show the boxed areas of the left and middle panels at shorter time scales. A brief laser pulse (1 ms) induces a ~10 mV IPSP in the tonic cell, but switches the bistable cell from its up-state to the down-state.

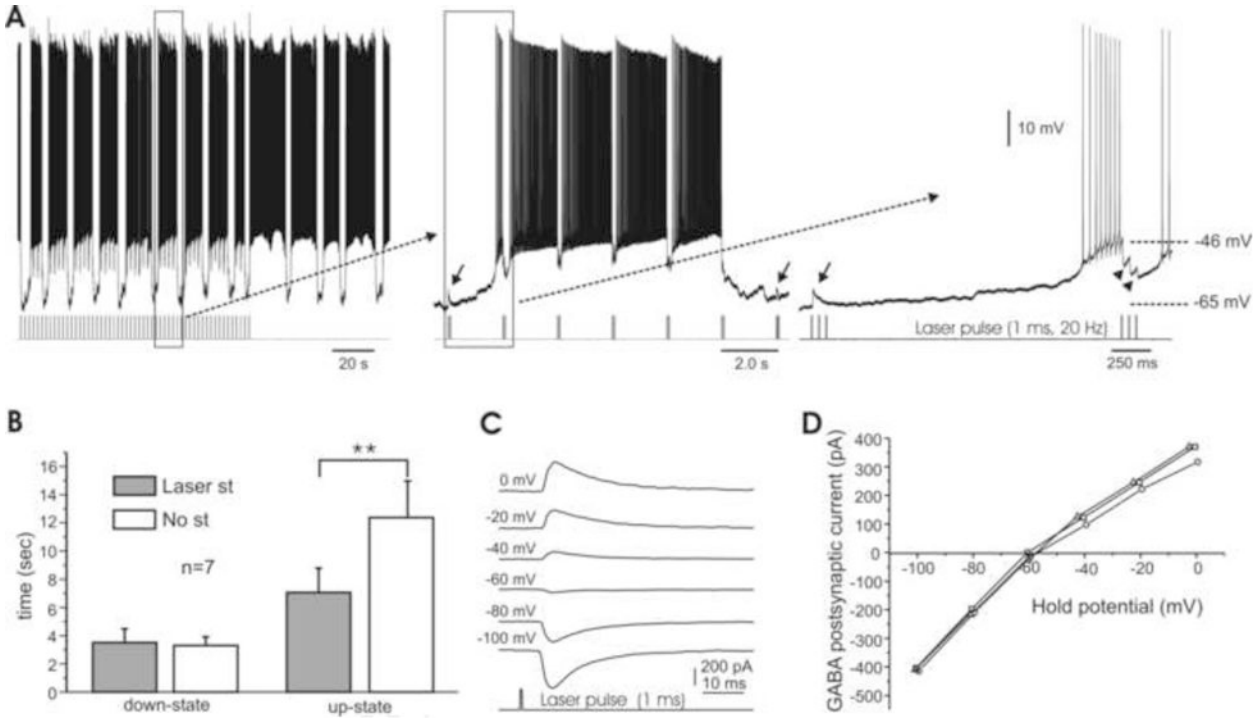

Fig. 9. Bidirectional modulations of DCN cell bursting by photostimulation-induced GABA release

A. A regular firing pattern persists under photo stimulation of 3 pulses at 20 Hz, delivered every 2s. However, upon removal of photostimulation the duration of the bursts lengthens (left). Time-expanded panels (middle, right) show that the laser pulses induce IPSPs (arrowheads) during up-states but EPSPs (arrows) during down-states. **B.** Bar graph of electrical behavior in bistable cells, showing that the length of the down-state is unaffected by tonic photostimulation, while the up-state's duration is significantly increased without light-activated inhibition. **C.** Examples of photostimulation-induced, GABA-mediated postsynaptic currents obtained at various holding potentials (shown on the left) in a DCN cell under perforated patch. The reversal potential for this cell was -58 mV. Note the delay (~5 ms) between the laser pulse and onset of current responses. **D.** I-V curves of three DCN cells, including the cell shown in E, with reversal potentials ranging from -58 to -62 mV.